Makara Journal of Science

Volume 26
Issue 1 *March*

Article 3

3-30-2022

An in Silico Study of the Cathepsin L Inhibitory Activity of Bioactive Compounds in Stachytarpheta jamaicensis as a Covid-19 Drug Therapy

Juliyatin Putri Utami
Department of Biomedicine, Faculty of Dentistry, Universitas Lambung Mangkurat, Banjarmasin, 70123 Indonesia, juliyatin.utami@ulm.ac.id

Nia Kurnianingsih
Department of Physiology, Faculty of Medicine, Universitas Brawijaya, Malang 65145, Indonesia

Mohammad Reza Faisal
Department of Computer Science, Faculty of Mathematics and Natural Sciences, Universitas Lambung Mangkurat, Banjarbaru 70714, Indonesia

Recommended Citation

Utami, Juliyatin Putri; Kurnianingsih, Nia; and Faisal, Mohammad Reza (2022) "An in Silico Study of the Cathepsin L Inhibitory Activity of Bioactive Compounds in Stachytarpheta jamaicensis as a Covid-19 Drug Therapy," *Makara Journal of Science*: Vol. 26: Iss. 1, Article 3.
DOI: 10.7454/mss.v26i1.1269
Available at: https://scholarhub.ui.ac.id/science/vol26/iss1/3

Makara Journal of Science, 26/1 (2022), 25–36
doi: 10.7454/mss.v26i1.1269

An in Silico Study of the Cathepsin L Inhibitory Activity of Bioactive Compounds in *Stachytarpheta jamaicensis* as a Covid-19 Drug Therapy

Juliyatin Putri Utami[1,2*], Nia Kurnianingsih[3,4], and Mohammad Reza Faisal[5]

1. Department of Biomedicine, Faculty of Dentistry, Universitas Lambung Mangkurat, Banjarmasin, 70123 Indonesia
2. Indonesian Genetics and Biodiversity Foundation, South Jakarta City, Jakarta 12540, Indonesia
3. Department of Physiology, Faculty of Medicine, Universitas Brawijaya, Malang 65145, Indonesia
4. Smart Molecule of Natural Genetics Resource Research Center, Universitas Brawijaya, Malang 65145, Indonesia
5. Department of Computer Science, Faculty of Mathematics and Natural Sciences, Universitas Lambung Mangkurat, Banjarbaru 70714, Indonesia

E-mail: juliyatin.utami@ulm.ac.id

Received August 10, 2021 | Accepted January 27, 2022

Abstract

Inhibition of cathepsin L (Cat L) can be considered a target for COVID-19 treatment. *Starchytapheta jamaicensis* is a plant from the Verbenaceae family that is commonly used for medicinal purposes. This study aims to analyze the inhibitory activities of compounds of *Stachytarpheta jamaicensis* toward Cat L by computational docking analysis. Ten compounds contained in the extracts (i.e., α-spinasterol, apigenin, luteolol-7-glucuronide, friedelin, hispidulin, chlorogenic acid, ipolamiide, geraniol, hentriacontane, and γ-aminobutyric acid) were selected as ligands; decanoyl-arg-val-lys-arg-chloromethylketone and oxocarbazate were used as the reference. Computational docking analysis was performed using Autodock Vina integrated into PyRx 8.0 and visualized using the Discovery Studio Visualizer v19.1.0.18287 (2019 version) based on the scoring functions. Seven bioactive compounds were bound more strongly than decanoyl-arg-val-lys-arg-chloromethylketone: α-spinasterol, apigenin, luteolol-7-glucuronide, friedelin, hispidulin, chlorogenic acid, and ipolamiide. However, all bioactive compounds were bound with less strength than oxocarbazate. Apigenin showed the best affinity, with much hydrogen bonding, and had the same ASN18 residue as Cat L inhibitor 1. PreADMET showed that all compounds of *S. jamaicensis* did not have hepatotoxicity, mutagenic, and carcinogenic criteria. The current research indicates that *S. jamaicensis* compounds can be used as an inhibitor for Cat L and as a COVID-19 drug candidate.

Keywords: active compounds, cathepsin L, COVID-19, SARS-CoV2, Stachytarpheta jamaicensis

Introduction

COVID-19 is an acute respiratory disease caused by a coronavirus (SARS-CoV-2) transmitted from animals to humans [1]. Viruses enter the human body through the respiratory system. The spike protein on the SARS-CoV-2 viral membrane interacts with the angiotensin-converting enzyme (ACE2) receptor to enter the host cells on the target cell surface [1, 2]. SARS-CoV-2 infection has a similar transmission mechanism to SARS-CoV [3]. SARS-CoV, mediated by protein S, increases the sensitivity to protease inhibitors, namely, leupeptin [4]. The potential targets of SARS-CoV antivirals can be divided into two categories: the target of the action, which is the human immune system or human cells, and the coronavirus itself [5]. Other compounds are usually attached to several cell receptors in the human immune system that can block the attachment between the SARS-CoV virus and target cells. The first step of SARS-CoV-2 infection is host cell invasion mediated by the spike (S) glycoprotein. Protein S is a glycosylated type 1 membrane protein consisting of S1 and S2 subunits. The N-terminal S1 subunit consists of a receptor-binding domain that mediates binding to host cell receptors, namely, ACE2 for SARS-CoV and SARS-CoV-2 [6].

SARS-CoV-2 uses ACE2 for entry and the serine protease TMPRSS2 for S protein priming [7]. SARS-CoV-2 entry has three stages: membrane fusion involving receptor binding, inducing a change in the shape of the S glycoprotein, activation of cathepsin L, and activation of membrane fusion through the endosome [4, 8]. Cathepsin L will mediate the cleavage of the spike glycoprotein S1 subunit on the surface of the coronavirus. The coronavirus requires this division to enter the human host cell. Next, the endosome membrane of the host cell and the virus will fuse, and then the viral RNA releases the next stage of replication. A cell-free membrane-fusion system exhibits

receptor binding followed by proteolysis, the action of cathepsin L [4].

Cathepsin L (Cat L) is one type of endosomal cysteine protease enzyme that assembles collagen from procollagen and plays a role in cell proliferation, namely, proteolytic control by cyclins [9]. In addition, this enzyme plays a role in physiological processes such as cell-matrix degradation in the inflammatory process, apoptosis, antigen processing, and MHC class II immune responses [10–12]. Elastolytic cysteine proteases are mobilized to the cell surface of macrophages and other cells under inflammatory conditions, which leads to accelerated collagen and elastin degradation, exacerbating inflammation and tissue damage [11, 12]. Cathepsin requires pH conditions between 4.5–5, which describe the state of lysosomes. The expression of this enzyme is usually expressed in various cell types and all tissues. It plays an essential role in the proteolysis of antigen proteins caused by the endocytosis of pathogens [9]. Previous studies showed inhibition of Cat L overexpression in SARS-CoV-2 pseudo-virus infection by administering Cat L inhibitors in vitro and in vivo [13, 14]. Thus, inhibition of Cat L can be considered a target for COVID-19 treatment. In silico molecular docking is used to predict the interaction between ligands (small molecules) and large molecules, such as proteins, enzymes, and carbohydrates, to predict the exchange's stability and spontaneity, which can be seen through the smaller free energy [15,16]. Molecular docking is often used to discover new drug candidates and study antigen and antibody interactions. Additionally, molecular docking is often used to find potential compounds that can act as work inhibitors of disease agents, such as viruses and bacteria [17, 18].

Throughout human history, herb species and fruits have served as sources of herbal medicine. They contain various phytochemicals, such as flavonoids, alkaloids, glucosides, and polyphenolic compounds. Secondary metabolites found in *S. jamaicensis* have a role as anti-cancer, anti-allergy, antioxidant, and anti-inflammatory agents and as an inhibitor of certain enzymes [19–21]. *S. jamaicensis* also has been used as a traditional medicine to cure allergies and problems with respiratory conditions, coughs, colds, fever, and digestive complications [22].

S. jamaicensis is a plant from the Verbenaceae family that grows in the tropics. Almost all parts of this plant can be used as medicine [23]. In general, the people of Kalimantan use this plant to treat sore throats and coughs. According to Liew (2015), *S. jamaicensis* contains secondary metabolites, such as flavonoids, phenols, saponins, tannins, and terpenoids [22].

S. jamaicensis contains glycosides, which are usually found only in Verbenaceae plants. In previous studies, Stachytarpheta species phytochemical screening revealed the presence of alkaloids, tannins, saponins, glycosides, steroids, and phenols [24–26]. The main plant chemicals in *S. jamaicensis* include apigenin-7-glucuronide, α-spinasterol, γ-aminobutyric acid, chlorogenic acid, citral, dopamine, friedelin, geraniol, hentriacontane, hispidulin, ipolamiide, luteolol-7-glucuronide, n-dotriacontane, n-nonacosane, n-pentriacontane, n-tetratriancontane, n-triacontane, n-tritriacontane, salicylic-acid, scutellarein, stachytarphine, stigmasterol, tarphetalin, ursolic acid, and verbascoside [27]. Lipinski's rule of five is used to predict the oral bioavailability of a drug-likeness of these compounds [28]. All compounds used in this simulation, namely, α-spinasterol, apigenin, luteolin-7-glucuronide, friedelin, hispidulin, chlorogenic acid, ipolamiide, geraniol, hentriacontane, and γ-aminobutyric acid, complied with Lipinski's rule.

The comparison ligands used in this study are inhibitor compounds that act directly on Cat L, namely, decanoyl-arg-val-lys-arg-chloromethyl ketone (Ddec-RVKR-CMK) and oxocarbazate [29–31]. This study predicts a therapeutic target for SARS-CoV-2 using 10 compounds from *Stachytarpheta jamaicensis* that may inhibit novel coronaviruses through cathepshin L inhibition and provides scientists with information on compounds that may be effective.

Methods

Data mining/ligand and protein sampling. The molecular docking receptor preparation 3D structure of Cat L (3K24) was taken from the Protein Data Bank (https://www.rcsb.org/). The preparation structure of the bioactive compound of *S. jamaicensis* and 3D structures of the ligand references (Ddec-RVKR-CMK and oxocarbazate) were downloaded from PubChem (https://pubchem.ncbi.nlm.nih.gov/). Protein structures were downloaded in.pdb format, while ligands were downloaded in SDF format.

Protein and ligand preparation. The compounds used were apigenol-7-glucuronide (CID 5319484), α-spinasterol (CID 5281331), γ-aminobutyric acid (CID 119), chlorogenic acid (CID 1794427), friedelin (CID 91472), geraniol (CID 637566), hentriacontane (CID 12410), hispidulin (CID 5281628), ipolamiide (CID 442425), and luteolol-7-glucuronide (CID 5280601). Molecular docking proteins were prepared using Discovery Studio version 16 (Dassault Systèmes BIOVIA, 2015) to remove previously attached ligands, while ligands were prepared using Open Babel integrated into PyRx 8.0 (Dallakyan & Olson, 2015) to minimize their energy and convert them to.pdb format [32].

Docking method validation. The docking method was validated by the redocking method using a natural ligand (2-acetamido-2-deoxy-beta-D-glucopyranose) (CID: 24139) with the prepared cathepsin L receptor [33]. In the docking validation process, the parameter is the RMSD

(root mean square deviation) value. The results of validating the native ligand with the cathepsin L receptor showed an RMSD value of 1.784 Å. The RMSD describes how much the protein–ligand interaction changes during docking to determine the deviation value. The docking method is valid if the value of RMSD ≤ 2 Å, which means that the docking parameter is valid, so that the docking method can be used to dock the test compound. This result showed that the docking method was valid and the setting parameters were validation criteria, so these parameters can be used for docking the test compound.

Docking of the protein–ligand and visualization. A molecular docking simulation was performed using Autodock Vina integrated into PyRx 8.0. Virtual prediction analysis and visualization of protein–ligand complexes from the docking step were analyzed and visualized using Discovery Studio. The interaction site was analyzed based on the ligand–residue interaction and structural conformation. Cat L was also docked with reference ligands to compare the binding affinity of the 10 active compounds used in this study according to previous research.

Drug-likeness, pharmacokinetic, and safety predictions. Lipinski's rule of 5 was used to predict the drug-likeness of bioactive compounds, which is evaluated by the free accessible website www.molinspiration.com. The pharmacokinetic and safety predictions were performed using a special program at http://biosig.unimelb.edu.au/pkcsm/. The pharmacokinetic parameters included absorption, distribution, and excretion.

Results and Discussion

Table 1 compares the physicochemical properties of the *S. jamaicensis* bioactive compounds with two native ligands. According to Lipinski's rule of 5, α-spinasterol, γ-aminobutyric acid, hispidulin, geraniol, friedelin, and hentriacontane are predicted to be favorable oral drug candidates because they have a molecular weight of less than 500, fewer than five hydrogen bond donors, and fewer than 10 hydrogen bond acceptors. However, according to the logP value, α-spinasterol, hispidulin, geraniol, friedelin, and hentriacontane are more complimentary because of their solubility in the aqueous phase.

According to the pharmacokinetic prediction (Table 2), most of the bioactive compounds of *S. jamaicensis* are well-absorbed in the human intestine, as the range of absorption was 70–100%, excluding apigenin, chlorogenic acid, luteolin, and ipolamiide. The highest absorbed compounds in Caco-2 cells were friedelin and α-spinasterol, at 1.27 and 1.21 log cm/s, respectively. The Caco-2 cells are an in vitro model for determining drug transport through intestinal epithelium derived from human colonic adenocarcinomas that have multiple transport pathways [34]. The data show that the permeability of the active compound to pass through the intestinal epithelium is still relatively small. This attribute can affect its bioavailability in the blood, so pharmaceutical or structural modification must be performed to increase the permeability properties of these compounds.

Table 1. Physicochemical Properties of *S. jamaicensis* Bioactive Compounds in Correlated with Lipinski's Rules

No	Ligand	Molecular Weight (g/mol)	logP	Hydrogen Bond Donor (n)	Hydrogen Bond Acceptor (n)	Molar Refractivity	TPSA
1	Decanoyl-arg-val-lys-arg-chloromethylketone	744.42	0.77	9	8	203.46	288.29
2	Oxocarbazate	535.60	3.34	4	6	147.85	141.86
3	Apigenin-7-glucuronide	446.40	0.14	6	10	106.72	178.47
4	α-Spinasterol	412.70	7.80	1	1	132.75	186.35
5	γ-Aminobutyric acid	103.12	−0.19	2	2	25.82	63.32
6	Chlorogenic acid	354.31	−0.65	6	8	83.50	164.75
7	Hispidulin	300.26	2.58	3	6	80.48	100.13
8	Luteolol-7-glucuronide	462.40	−0.15	7	11	108.74	207.35
9	Geraniol	154.25	2.67	1	1	50.40	20.23
10	Friedelin	426.70	8.46	0	1	134.39	17.07
11	Ipolamiide	406.40	−2.89	6	11	88.60	175.37
12	Hentriacontane	436.80	12.30	0	0	151.13	0.00

Table 2. Pharmacokinetic Prediction of *S. jamaicensis* Bioactive Compounds by ADMET

No.	Ligand	Caco-2 ($nm.sec^{-1}$)	Human intestinal absorption (%)	VDss (log L/kg)	CYP2D6 Inhibitor	Total Clearance (log mL/min/kg)
1	Decanoyl-arg-val-lys-arg-chloromethylketone	0.35	8.62	−0.74	No	0.32
2	Oxocarbazate	0.25	70.64	−0.35	No	−0.02
3	Apigenin-7-glucuronide	−0.69	15.26	0.32	No	0.59
4	α-Spinasterol	1.21	94.97	0.77	No	0.61
5	γ-Aminobutyric acid	0.58	77.81	−0.65	No	0.57
6	Chlorogenic acid	−0.84	36.38	0.58	No	0.31
7	Hispidulin	−0.04	84.65	0.37	No	0.53
8	Luteolol-7-glucuronide	−0.89	15.20	0.86	No	0.52
9	Geraniol	1.49	92.79	0.17	No	0.44
10	Friedelin	1.27	98.74	−0.27	No	−0.04
11	Ipolamiide	0.43	27.52	0.18	No	1.27
12	Hentriacontane	1.10	85.89	−0.02	No	2.19

According to the pharmacokinetic prediction (Table 2), most of the bioactive compounds of *S. jamaicensis* are well-absorbed in the human intestine, as the range of absorption was 70–100%, excluding apigenin, chlorogenic acid, luteolin, and ipolamiide. The highest absorbed compounds in Caco-2 cells were friedelin and α-spinasterol, at 1.27 and 1.21 log cm/s, respectively. The Caco-2 cells are an in vitro model for determining drug transport through intestinal epithelium derived from human colonic adenocarcinomas that have multiple transport pathways [34]. The data show that the permeability of the active compound to pass through the intestinal epithelium is still relatively small. This attribute can affect its bioavailability in the blood, so pharmaceutical or structural modification must be performed to increase the permeability properties of these compounds.

The distribution phases, the second phase of pharmacokinetics, may interact with each other, known by the volume of distribution (VDss). α-Spinastrol and luteolol-7-glucuronide had a range of VDss values (between 0.71 L/kg and 2.81 L/kg), which were higher than those of other compounds. Many drugs are bound to proteins in the plasma and make an ineffective form, and the free plasma concentration of a drug is active. A balancing between bound and unbound forms of a drug occurs. When free unbound drugs are excreted, some drugs displace other drugs from their proteins, increasing the free, unbound concentration in the plasma, which leads to side effects [35]. The VDss considers seeing the potential toxicity of a drug. The third drug pharmacokinetics phase is hepatic metabolism. Almost all available drugs are metabolized by CYP450 enzymes [36]. This study showed that all compounds have no inhibition against the CYP450 enzyme, thus the pharmacokinetics prediction was enzymatic.

A safety prediction of all bioactive compounds was made by determining the acute and chronic lethal dosages as LD50 and LOAEL, respectively (Table 3). A toxicity prediction demonstrated that apigenin, α-spinasterol, luteolin, and friedelin have a higher LD50 than the reference ligand compound. Prediction of toxicity through the same site, using the Ames test method, is a simple way to test the properties of compounds in the form of mutagenic and carcinogenic properties as frameshift mutagens [37,38]. The prediction result data indicate that all active compounds of *S. jamaicensis* are neither mutagenic nor carcinogenic. Likewise, the hepatoxicity test results showed that none of the ligands of the active compound *S. jamaicensis* induced liver damage. However, the hepatotoxicity results indicate that the reference ligand compound has the potential to cause liver damage, so the toxicity data of the tested ligand are better than those of the reference ligand.

Table 3. Toxicity and Safety Predictions of *S. jamaicensis* Compounds and Reference Ligands by ADMET

No.	Ligand	AMES toxicity	Hepatotoxicity	Oral Rat Acute Toxicity (LD50) (mol/kg)	Oral Rat Chronic Toxicity (LOAEL) (log mg/kg_bw/day)
1	Decanoyl-arg-val-lys-arg-chloromethylketone	No	Yes	2.48	2.82
2	Oxocarbazate	No	Yes	2.37	3.70
3	Apigenin-7-glucuronide	No	No	2.64	4.40
4	α-Spinasterol	No	No	2.54	0.87
5	γ-Aminobutyric acid	No	No	1.64	2.93
6	Chlorogenic acid	No	No	1.97	2.98
7	Hispidulin	No	No	2.40	1.63
8	Luteolol-7-glucuronide	No	No	2.56	4.30
9	Geraniol	No	No	1.64	2.03
10	Friedelin	No	No	2.64	0.91
11	Ipolamiide	No	No	2.23	3.42
12	Hentriacontane	No	No	1.86	0.85

Table 4 shows the binding capacity of *S. Jamaicensis* bioactive compounds on Cat L as an enzyme related to the COVID-19 cycle in humans. The binding energy of the 10 bioactive compounds varied from −4.2 to −8.9 kcal/mol. Seven bioactive compounds were more strongly bound than decanoyl-arg-val-lys-arg-chloromethyl ketone as an inhibitor of Cat L, namely, α-spinasterol, apigenin- and luteolol-7-glucuronide, friedelin, hispidulin, chlorogenic acid, and ipolamiide. However, all the bioactive compounds were less strongly bound than oxocarbazate as the second inhibitor of Cat L. The binding interaction value has the potential to predict the interaction strength between ligand and receptor, as a more negative value indicates a stronger binding interaction [32]. The energy values provide an approximate estimate of the ease of formation, the relief of disruption, and the relative strengths of various intermolecular interaction types [39].

Although the bioactive compounds of *S. jamaicensis* have a weaker binding interaction than oxocarbazate, geraniol has the most similar hydrogen bond interaction with oxocarbazate at residues PRO15, ARG8, and VAL13. A less similar interaction was demonstrated between oxocarbazate and chlorogenic acid, followed by hentriacontane and hispidulin. Meanwhile, the bioactive compounds of apigenin, α-spinasterol, chlorogenic acid, hispidulin, and luteolol-7-glucoronide have one hydrogen bond interaction similar with decanoyl-arg-val-lys-arg-chloromethylketone.

Hydrogen bonding is a principle protein–ligand interaction. This bond provides stronger affinity, thus it is crucial in drug design development [40]. Intramolecular hydrogen bonds have considerable importance in stabilizing structures [39]. Hispidulin was the compound ligand and Cat L complex with the most hydrogen bonds. Meanwhile, hentriacontane had the most hydrophobic bonds. Hydrophobic binding plays a vital role in stabilizing the conformation of proteins, transporting lipids by plasma proteins, and binding steroids to their receptors, among other examples [39].

Apigenin–Cat L complex interactions were through carbon-hydrogen bonds, conventional hydrogen bonds, pi-pi stacking, and pi-alkyl formation. The binding energy of the apigenin–Cat L complex was −8.7 kcal/mol. The docking energy generated from the interaction between α-spinasterol and Cat L was −8.9 kcal/mol. Six bonds were formed in this interaction (Figure 1d). Hydrogen bonds occurred at GLU148 and GLU192 on the OH groups of ligand molecules. Hydrophobic bonds involved HIS163, TRP189, and TRP193.

γ-Aminobutyric acid was observed to bind to the Cat L site with −4.2 kcal/mol (Figure 1e). The γ-aminobutyric acid–Cat L complex had weaker interactions than the complexes of other ligands (Table 2). On the basis of the molecular docking results shown in Table 2, amino acid residues bonded to γ-aminobutyric acid through conventional hydrogen bonds.

The chlorogenic acid–Cat L complex had more interactions than the complexes of γ-aminobutyric, geraniol, ipolamiide, and hetriacontane based on the molecular docking results shown in Figure 1. There are three hydrogen bonds between the chlorogenic acid ligand and Cat L and a −8.2 kcal/mol binding energy with ARG8, TYR198, and GLU191. Conversely, PRO15, ARG8, and VAL13 mediated pi-alkyl and amide pi-stacking through hydrophobic interactions. The amino acid residue VAL13 interacted with this ligand through other bonds.

Table 4. Comparison of the Binding Energy of Compound Ligands and Reference Ligands with Cat L

Hydrogen Bond Interaction			
Compound	**Docking Score (kcal/mol)**	**Amino residues (Interaction Type)**	**Distance (Å)**
Decanoyl-arg-val-lys-arg-chloromethylketone (Ddec-RVKR-CMK) (Inhibitor 1)	−5.6	GLU192 (Electrostatic)	4.3
		TYR182 (Conventional)	2.3
		ASN18 (Conventional)	2.9
		GLU191 (Conventional)	2.4
		TYR170 (Conventional)	3.07
		TYR182 (Conventional)	2.7
		ASP6 (Conventional)	2.5
		GLU9 (Conventional)	3.04
		GLU50 (Conventional)	3.03
		GLU86 (Conventional)	2.9
		PHE172 (Pi-Alkyl)	4.9
Oxocarbazate (Inhibitor 2)	−11	ASP6 (Attractive)	4.5
		GLU9 (Attractive)	4.7
		GLU191 (Conventional)	2.5
		VAL16 (Conventional)	2.9
		TYR182 (Pi-Donor)	3.9
		ARG8 (Alkyl)	4.8
		ARG8 (Alkyl)	4.7
		PRO15 (Alkyl)	4.5
		PRO15 (Alkyl)	5.02
		VAL13 (Alkyl)	5.4
		LEU184 (Alkyl)	5.3
Apigenin-7-glucuronide	−8.7	GLN19 (Conventional)	2.8
		ASP162 (Conventional)	2.4
		ASN18 (Conventional)	2.3
		LEU144 (Conventional)	2.6
		GLY23 (Carbon)	3.4
		TRP 189 (Pi-Pi Stacked)	3.5
		LEU144 (Pi-Alkyl)	5.04
α-Spinasterol	−8.9	GLU148 (Conventional)	2.6
		GLU192 (Conventional)	2.4
		TRP189 (Pi-Sigma)	3.6
		HIS163 (Pi-Alkyl)	5.04
		TRP189 (Pi-Alkyl)	3.7
		TRP193 (Pi-Alkyl)	5.3
γ-Aminobutyric acid	−4.2	GLY196 (Conventional)	3.01
		GLU192 (Conventional)	2.6
		TRP193 (Conventional)	2.4
		GLY194 (Conventional)	2.1
		LYS147 (Conventional)	2.3

Table 4. Comparison of the Binding Energy of Compound Ligands and Reference Ligands with Cat L (*Continue*)

Hydrogen Bond Interaction			
Compound	**Docking Score (kcal/mol)**	**Amino residues (Interaction Type)**	**Distance (Å)**
Chlorogenic acid	−8.2	ARG8 (Conventional)	2.8
		TYR198 (Conventional)	2.7
		GLU191 (Conventional)	2.1
		ARG8 (Carbon)	3.3
		VAL13 (Pi Lone Pair)	2.9
		THR14 (Amide Pi-Stacked)	4.9
		PRO15 (Pi-Alkyl)	3.7
		ARG8 (Pi-Alkyl)	5.02
		VAL13 (Pi-Alkyl)	5.3
Hispidulin	−8.6	ARG8 (Conventional)	2.9
		GLY191 (Conventional)	2.4
		GLU191 (Conventional)	2.1
		MET195 (Carbon)	3.3
		GLY196 (Carbon)	3.5
		THR14 (Amide Pi-Stacked)	4.7
		TYR198 (Conventional)	4.9
		PRO15 (Pi-Alkyl)	3.6
		VAL16 (Pi-Alkyl)	5.02
		ARG8 (Pi-Alkyl)	4.8
		VAL13 (Pi-Alkyl)	5.3
Luteolol-7-glucuronide	−8.7	GLY164 (Conventional)	3.25
		ASN18 (Conventional)	1.86
		HIS163 (Carbon)	3.2
		ASP162 (Carbon)	3.3
		TRP189 (Pi- Pi Stacked)	3.9
Geraniol	−5.5	MET195 (Conventional)	2.4
		GLY196 (Carbon)	3.3
		PRO15 (Alkyl)	4.8
		ARG8 (Alkyl)	3.8
		VAL13 (Alkyl)	4.4
Friedelin	−8.7	LYS147 (Conventional)	2.9
Ipolamiide	−7.3	GLN19 (Conventional)	3.3
		TRP26 (Conventional)	3.3
		GLY164 (Conventional)	3.2
		GLY68 (Conventional)	2.4
		TRP26 (Carbon)	3.5
Hentriacontane	−4.3	PRO90 (Alkyl)	5.4
		LYS17 (Alkyl)	3.7
		VAL5 (Alkyl)	4
		LYS10 (Alkyl)	4.9
		PRO15 (Alkyl)	3.9
		TYR91 (Alkyl)	4.9

Three conventional hydrogen bonds and two carbon-hydrogen bonds were formed between hispidulin and Cat L protein (Figure 1g). The amino acid residues involved in hydrogen bond formation were ARG8, GLY191, GLU191, MET195, and GLY196. Six amino acid residues, namely, THR14, TYR198, PRO15, VAL16, ARG8, and VAL13, formed hydrophobic interactions with hispidulin. The binding energy of the hispidulin–Cat

L complex was −8.6 kcal/mol. The luteolol-7-glucuronide–Cat L complex and friedelin–Cat L complex had slightly more interactions than the hispidulin–Cat L complex, resulting in a −8.7 kcal/mol binding energy (Table 4). On the basis of the molecular docking results shown in Figure 1h, GLY164, ASN18, HIS163, and ASP162 formed hydrogen bonds with luteolin. Only TRP189 interacted with luteolin through pi-pi stacked hydrophobic bonds (Figure 1h). In comparison, only LYS147 of the friedelin–Cat L complex had a conventional hydrogen bond (Figure 1j). Five interactions were facilitated by carbon-hydrogen bonding, conventional hydrogen bonding, and alkyl formation in the geraniol-Cat L complex shown in Figure 1i. Two hydrogen bonds were formed by MET195 (conventional) and GLY196 (carbon). PRO15, ARG8, and VAL13 formed hydrophobic bonds. The binding energy of this complex was −5.5 kcal/mol.

The binding energy of the ipolamiide–Cat L complex was −7.3 kcal/mol, higher than the complexes of geraniol, γ-aminobutyric, hentriacontane, and inhibitor 1. GLN19, TRP26, GLY164, GLY68, and TRP 26 interacted with ipolamiide through conventional hydrogen bonds and carbon-hydrogen bonds (Figure 1k). The last docking compound of *S. jamaicensis* was hentriacontane. This ligand had a −4.3 kcal/mol binding energy, which was similar to the γ-aminobutyric binding energy (Table 1), despite differences in amino acid residues. The hentriacontane-Cat L complex had six amino residues, namely, PRO90, LYS17, VAL5, LYS10, PRO15, and TYR91. They bonded to hentriacontane through alkyl hydrophobic bonds (Figure 1l).

Although α-spinasterol had the highest binding energy, it did not have the same amino acid residues as inhibitor 1 and inhibitor 2. Among all compounds, apigenin showed the best affinity, with many hydrogen bonds, and it had the same ASN18 residue as inhibitor 1 of Cat L. Apigenin's affinity and interaction with Cat L was even better than that of inhibitor 1. α-Spinasterol had the highest binding energy, and its amino acid residues differed from those of inhibitor 1 and inhibitor 2. Among all the tested *S. jamaicensis* compounds, apigenin showed the best affinity, with many hydrogen bonds, and had the same ASN18 residue as the Cat L inhibitor 1. Apigenin's affinity and interaction with Cat L was even better than that of inhibitor 1.

A. Cat L- Decanoyl-arg-val-lys-arg-chloromethylketone

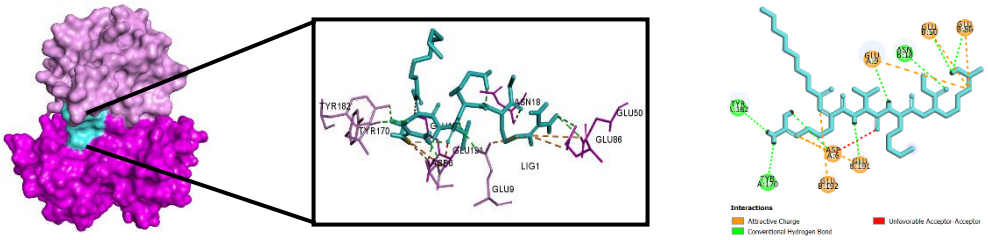

B. Cat L- Oxocarbazate

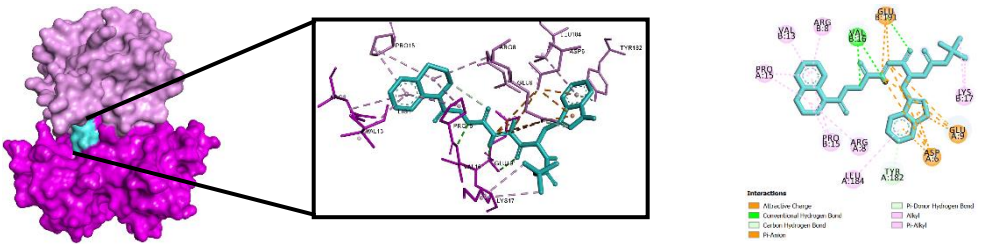

C. Cat L-Apigenin

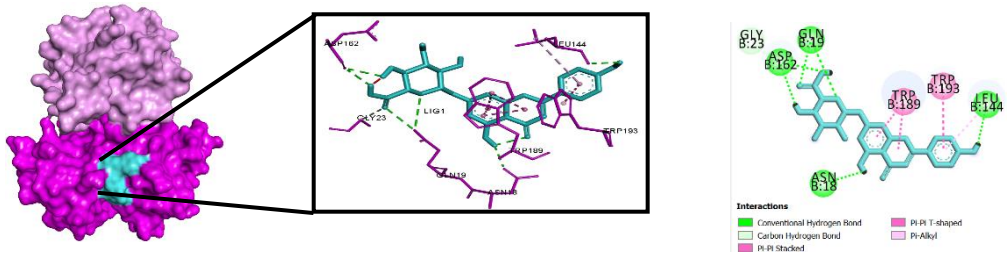

D. Cat L-α Sitosterol

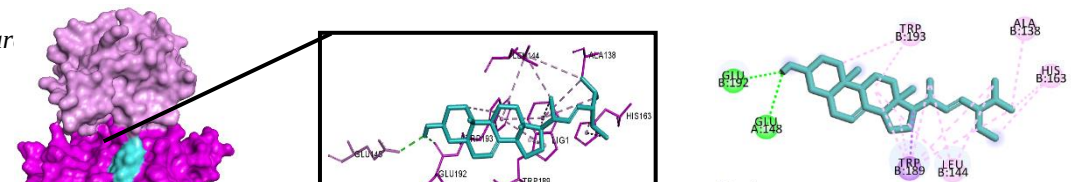

E. Cat L-γ Butyric acid

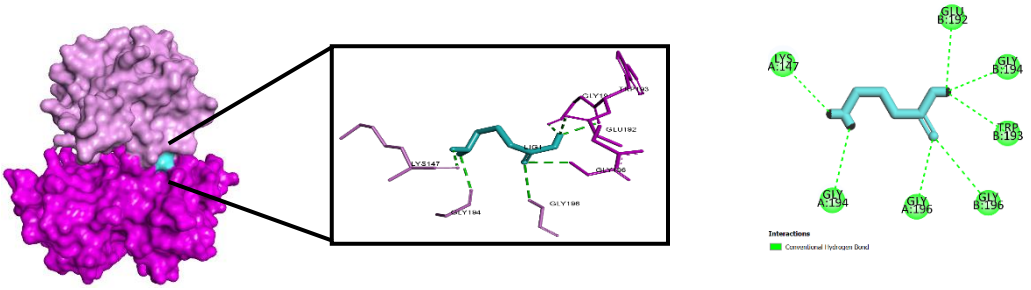

F. Cat L-Chlorogenic acid

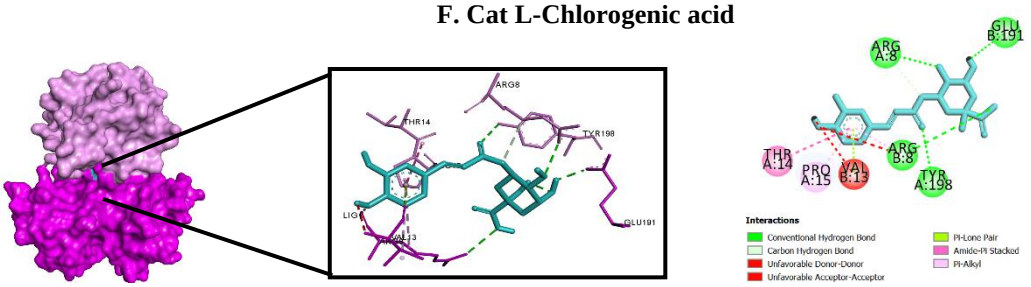

G. Cat L-Hispidulin

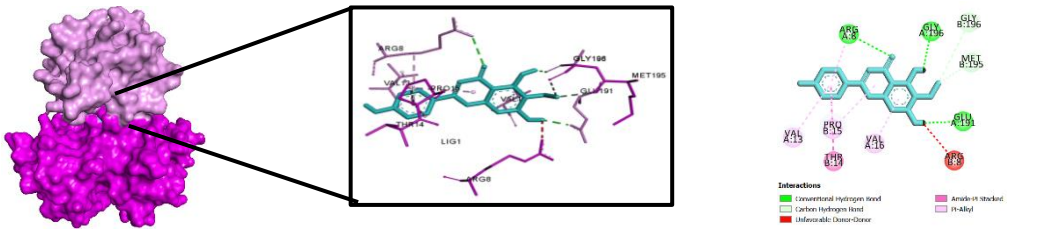

H. Cat L-Luteolol

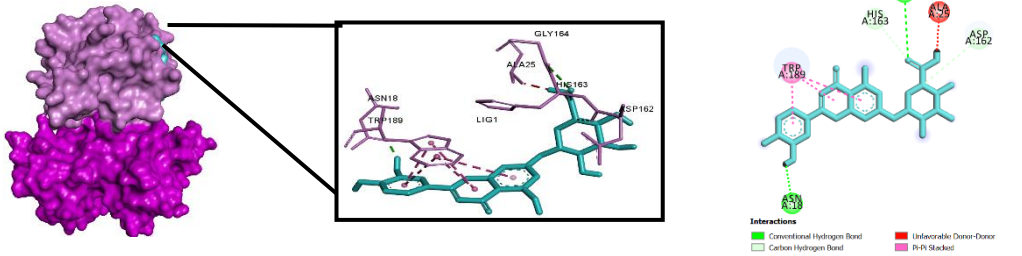

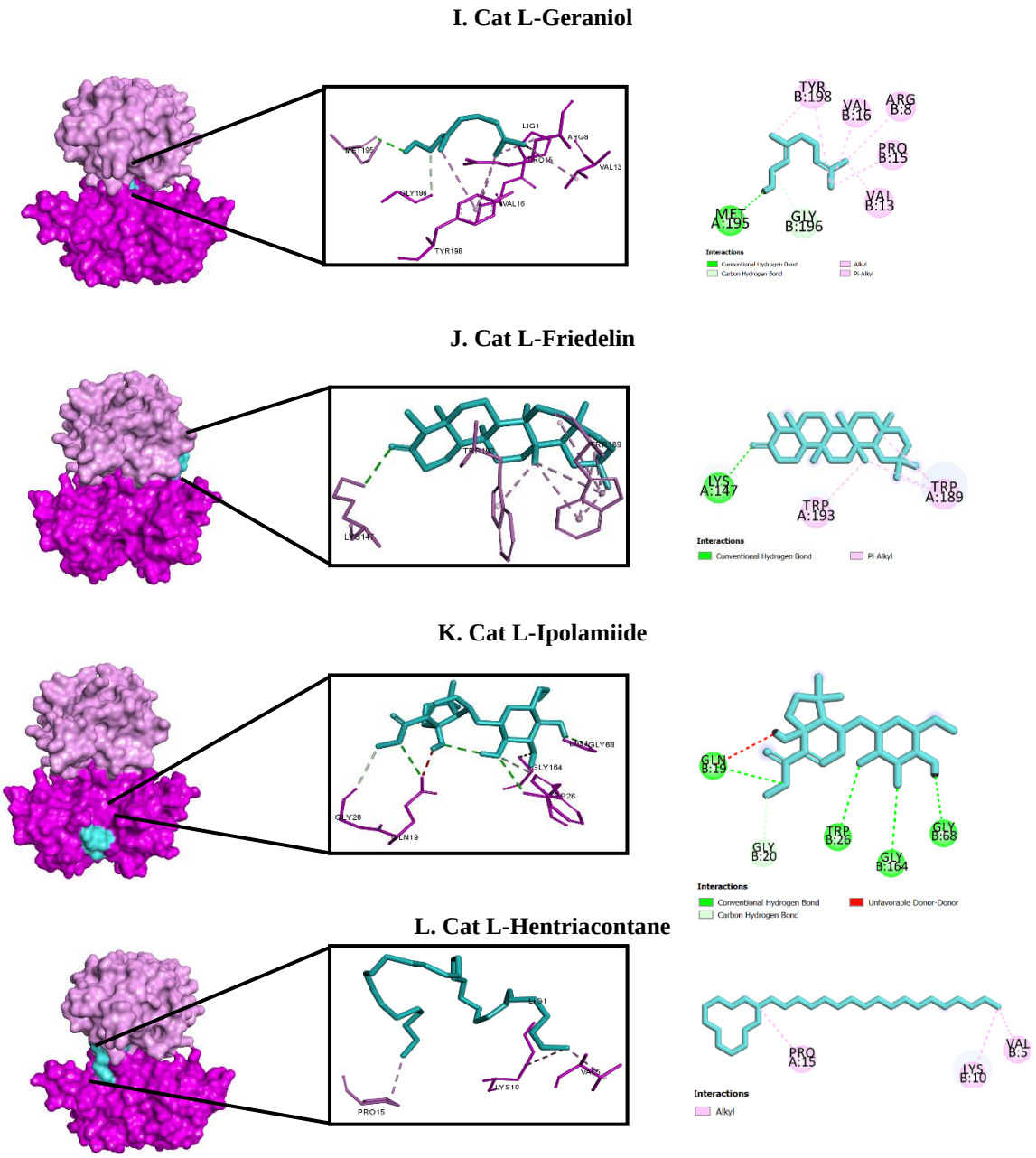

Figure 1. 3D Structures of the Interaction between *S. jamaicensis* Compounds (Turquoise) and the Cat L Receptor (Purple – Fuschia). Left and Center Sides Show the 3D Structure of the Interaction, While the Coded Right Side is the 2D Interaction and Category Bond of the Complex. Molecular Docking was Performed using Pyrx 8.0.0 Software and Visualization was Analyzed by the Discovery Studio Visualizer v19.1.0.18287 Program

Conclusion

In silico molecular docking studies obtained the models of the interactions between the ligands and the cathepsin L protein. The interactions between this protein and the ligands used in this study help us to understand the potential mechanisms of their interactions. Most of the bioactive compounds of *S. jamaicensis* were predicted to be well-absorbed in the human intestine, excluding apigenin, chlorogenic acid, luteolin, and ipolamiide. α-Spinasterol has the strongest binding affinity (−8.9 kcal/mol) followed by apigenin (−8,7 kcal/mol), luteolol-7-glucuronide (−8.7 kcal/mol), friedelin (−8.7 kcal/mol), hispidulin (−8.6 kcal/mol), chlorogenic acid (−8.2 kcal/mol), ipolamiide (−7.3 kcal/mol), geraniol (−5.5 kcal/mol), hentriacontane (−4.3 kcal/mol), and γ-aminobutyric acid (−4.2 kcal/mol). However, none of the compounds was higher than oxocarbazate (−11 kcal/mol). The ligand test showed that ASN18, PRO15, and VAL13 have the same interaction as the reference ligands. Thus, the most potent inhibitor of cathepsin L was apigenin. This study showed that *S. Jamaicensis*

could be used as an inhibitor for Cat L and as a COVID-19 drug candidate. Nonetheless, further studies are needed to support this modeling study through biological functions exploration in vivo and in vitro using the SARS-CoV-2 peptide.

Conflict of Interest

The authors of this work have no conflicts of interest.

Acknowledgements

The authors thank Indonesian Genetics and Biodiversity Foundation, the Faculty of Dentistry at the University of Lambung Mangkurat, and the Faculty of Medicine at Universitas Brawijaya, which have supported this work.

References

[1] Devaux, C.A., Rolain, J.M., Raoult, D. 2020. ACE2 receptor polymorphism: Susceptibility to SARS-CoV-2, hypertension, multi-organ failure, and COVID-19 disease outcome. J. Micro. Immunol. Infect. 53(3): 425–435, https://doi.org/ 10.1016/j.jmii.2020.04.015.

[2] Pitakbut, T. 2020. The antiviral activity of andrographolide, the active metabolite from andrographis paniculata (Burm. f.) wall. ex nees. against sars-cov-2 by using bio-and chemo-informatic tools. Walailak J. Sci. Technol. 17(8): 851–866, https://doi.org/10.48048/wjst.202 0.9728.

[3] Walls, A.C., Park, Y.J., Tortorici, M.A., Wall, A., McGuire, A.T., Veesler, D. 2020. Structure, Function, and Antigenicity of the SARS-CoV-2 Spike Glycoprotein. Cell. 181(2): P281–292.E6, https://doi.org/10.1016/j.cell.2020.02.058.

[4] Simmons, G., Gosalia, D.N., Rennekamp, A.J., Reeves, J.D., Diamond, S.L., Bates, P. 2005. Inhibitors of cathepsin L prevent severe acute respiratory syndrome coronavirus entry. Proc. Nat. Acad. Sci. US Am. 102(33), https://doi.org/ 10.1073/pnas.0505577102.

[5] Wu, C., Liu, Y., Yang, Y., Zhang, P., Zhong, W., Wang, Y., *et al*. 2020. Analysis of therapeutic targets for SARS-CoV-2 and discovery of potential drugs by computational methods. Acta Pharm. Sin. B 10(5): 766–788, https://doi.org/10.1016/ j.apsb.2020.02.008.

[6] Feng, W., Zong, W., Wang, F., Ju, S. 2020. Severe acute respiratory syndrome coronavirus 2 (SARS-CoV-2): A review. Mol. Canc. 19: 100, https://doi.org/10.1186/s12943-020-01218-1.

[7] Hoffmann, M., Kleine-Weber, H., Schroeder, S., Krüger, N., Herrler, T., Erichsen, S., *et al*. 2020. SARS-CoV-2 Cell Entry Depends on ACE2 and TMPRSS2 and Is Blocked by a Clinically Proven Protease Inhibitor. Cell. 181(2): P271–280.E8, https://doi.org/10.1016/j.cell.2020.02.052.

[8] Bittmann, S., Weissenstein, A., Villalon, G., Moschuring-Alieva, E., Luchter, E. 2020. Simultaneous Treatment of COVID-19 With Serine Protease Inhibitor Camostat and/or Cathepsin L Inhibitor? J. Clin. Med. Res. 12(5): 320–322, https://doi.org/10.14740/jocmr4161.

[9] Gomes, C.P., Fernandes, D.E., Casimiro, F., da Mata, G.F., Passos, M.T., Varela, P., *et al*. 2020. Cathepsin L in COVID-19: From Pharmacological Evidences to Genetics. Frontiers Cell. Infect. Microbiol. 10, https://doi.org/10.3389/fcimb.2020.5 89505.

[10] Hardiany, N.S. 2013. Cathepsin dan Calpain: Enzim Pemecah Protein dalam Sel. EJournal Kedokteran Indonesia. 1(1): 75–81, https://doi.org/ 10.23886/ejki.1.1602.75-83.

[11] Cao, Y., Liu, X., Li, Y., Lu, Y., Zhong, H., Jiang, W., *et al*. 2017. Cathepsin L activity correlates with proteinuria in chronic kidney disease in humans. Int. Urol. Nephrol. 49: 1409–1417, https://doi.org/ 10.1007/s11255-017-1626-7.

[12] Liu, T., Luo, S., Libby, P., Shi, G.P. 2020. Cathepsin L-selective inhibitors: A potentially promising treatment for COVID-19 patients. Pharmacol. Ther. 213: 107587, https://doi.org/ 10.1016/j.pharmthera.2 020.107587.

[13] Liu, C.L., Guo, J., Zhang, X., Sukhova, G.K., Libby, P., Shi, G.P. 2018. Cysteine protease cathepsins in cardiovascular disease: From basic research to clinical trials. Nat. Rev. Cardiol. 15: 351– 370, https://doi.org/10.1038/s41569-018-0002-3.

[14] Zhao, M.M., Yang, W.L., Yang, F.Y., Zhang, L., Huang, W.J., Hou, W., *et al*. 2021. Cathepsin L plays a key role in SARS-CoV-2 infection in humans and humanized mice and is a promising target for new drug development. Sign. Transduction Targeted Ther. 6(34), https://doi.org/ 10.1038/s41392-021-00558-8.

[15] Meng, X.-Y., Zhang, H.-X., Mezei, M., Cui, M. 2012. Molecular Docking: A Powerful Approach for Structure-Based Drug Discovery. Curr. Comput. Aided-Drug Des. 7(2): 146–157, https://doi.org/ 10.2 174/157340911795677602.

[16] Pedotti, M., Simonelli, L., Livoti, E., Varani, L. 2011. Computational docking of antibody-antigen complexes, oppotunities and pitfalls illustrated by influenza hemagglutinin. Int. J. Mol. Sci. 12(1): 226–251, https://doi.org/10.3390/ijms12010226.

[17] Kumar, Y., Singh, H., Patel, C.N. 2020. In silico prediction of potential inhibitors for the main protease of SARS-CoV-2 using molecular docking and dynamics simulation based drug-repurposing. J. Infect. Pub. Health. 13(9): 1210–1223, https://doi.org/10.1016/j.jiph.2020.06.016.

[18] Saddala, M.S., Adi, P.K.J., A, U.R. 2016. In Silico Drug Design and Molecular Docking Studies of Potent Inhibitors against Cathepsin-L (Ctsl) for Sars Disease. J. Res. Dev. 4(2): 1000145, https://doi.org/10.4172/2311-3278.1000145.

[19] de Souza, P.A., Silva, C.G., Machado, B.R.P., de Lucas, N.C., Leitão, G.G., Eleutherio, E.C.A., *et al*. 2010. Evaluation of antimicrobial, antioxidant and phototoxic activities of extracts and isolated compounds from Stachytarpheta cayennensis (Rich.) Vahl, Verbenaceae. Rev. Bras. Farmacognosia 20(6), https://doi.org/10.1590/S0102-695X2010005000042.

[20] Akuodor, C.G., Udia, M.P., Udenze, C.E., Ogbonna, J.O. 2013. Antibacterial Potential of the Methanol Stem Bark Extract of Stachytarpheta Indica. Asian J. Med. Sci. 4(4): 15–10, https://doi.org/10.3126/ajms.v4i4.8248.

[21] Zs, O., Oo, O., Se, K., Oo, A. 2017. *Stachytarpheta jamaicensis* leaf extract: Chemical composition, antioxidant, anti-arthritic, anti-inflammatory and bactericidal potentials. J. Sci. Innovative Res. 6(4): 119–125.

[22] Liew, P.M., Yong, Y.K. 2016. *Stachytarpheta jamaicensis* (L.) Vahl: From Traditional Usage to Pharmacological Evidence. Evidence-Based Complem. Alternative Med. 2016: 7842340, https://doi.org/10.1155/2016/7842340.

[23] Rizaldy, M.D., Hidajati, N. 2020. Isolasi Senyawa Metabolit Sekunder Dari Ekstrak Etil Asetat Daun Tanaman Pecut Kuda (*Stachytarpheta Jamaicensis*). Unesa J. Chem. 9(1): 23–28.

[24] Ruma, O.C. 2016. Antimicrobial Activity and Phytochemical Screening of Selected Indigenous Food Plants from Isabela, Philippines. Upland Farm J. 23.

[25] Calista, Tjipto, M.S., Putro, J.N., Nugraha, A.T., Soetaredjo, F.E., Ju, Y.H., *et al*. 2016. Supercritical CO2 extraction of bioactive compounds from *Stachytarpheta jamaicensis* (L) Vahl. Int. Food Res. J. 23(5): 2144–2150.

[26] Chinonye, I.I., Lynda, O.U., Adanna, U.A., Rita, O.N. 2019. Phytochemical, Antimicrobial and Gc/Ms Analysis of the Root of Stachytarpheta Cayennensis (L .Vahl) Grown in Eastern Nigeria. Eur.-Am. J. 7(2): 20–32.

[27] Herbal Secrets of the Rainforest. 2002–2003. Technical Data Report for GERVÂO *Stachytarpheta jamaicensis* Stachytarpheta cayennensis, 2nd ed. Leslie Taylor Gervâo, Sage Press, Inc.

[28] de Brito, M.A. 2011. Pharmacokinetic study with computational tools in the medicinal chemistry course. Braz. J. Pharm. Sci. 47(4), https://doi.org/10.1590/S1984-82502011000400017.

[29] Matsuyama, S., Shirato, K., Kawase, M., Terada, Y., Kawachi, K., Fukushi, S., *et al*. 2018. Middle East Respiratory Syndrome Coronavirus Spike Protein Is Not Activated Directly by Cellular Furin during Viral Entry into Target Cells. J. Virol. 92(19), https://doi.org/10.1128/jvi.00683-18.

[30] Mille, J.K., Whittaker, G.R. 2014. Host cell entry of Middle East respiratory syndrome coronavirus after two-step, furin-mediated activation of the spike protein. Proc. Nat. Acad. Sci. US Am. 111(42), https://doi.org/10.1073/pnas.1407087111.

[31] Shah, P.P., Wang, T., Kaletsky, R.L., Myers, M.C., Purvis, J.E., Jing, H., *et al*. 2010. A small-molecule oxocarbazate inhibitor of human cathepsin L blocks severe acute respiratory syndrome and ebola pseudotype virus infection into human embryonic kidney 293T cells. Mol. Pharm. 78(2): 319–324, https://doi.org/10.1124/mol.110.064261.

[32] Dallakyan, S., Olson, A.J. 2015. Small-molecule library screening by docking with PyRx. Method Mol. Biol. 1263: 243–250, https://doi.org/10.1007/978-1-4939-2269-7_19.

[33] van Meel, E., Lee, W.S., Liu, L., Qian, Y., Doray, B., Kornfeld, S. 2016. Multiple domains of GlcNAc-1-phosphotransferase mediate recognition of lysosomal enzymes. J. Biol. Chem. 291(15): P8295–8307, https://doi.org/10.1074/jbc.M116. 714568.

[34] Bollish, S.J. 1981. Applied Biopharmaceutics and Pharmacokinetics. Am. J. Health-System Pharm. 38(9): 1400–1404, https://doi.org/10.1093/ajhp/38.9.1400.

[35] Alshammari, T.M. 2016. Drug safety: The concept, inception and its importance in patients' health. Saudi Pharm. J. 24(4): 405–412, https://doi.org/10.1016/j.jsps.2014.04.008.

[36] Deodhar, M., al Rihani, S.B., Arwood, M.J., Darakjian, L., Dow, P., Turgeon, J., *et al*. 2020. Mechanisms of cyp450 inhibition: Understanding drug-drug interactions due to mechanism-based inhibition in clinical practice. Pharm. 12(9): 846, https://doi.org/10.3390/pharmaceutics12090846.

[37] Nursamsiar, Toding, A.T., Awaluddin, A. 2016. Studi In Silico Senyawa Turunan Analog Kalkon Dan Pirimidin Sebagai Antiinflamasi: Prediksi Absorpsi, Distribusi, dan Toksisitas. Pharmacy. 13(1): 92–100, https://doi.org/10.30595/pji.v13i1.891.

[38] Hsu, K.H., Su, B.H., Tu, Y.S., Lin, O.A., Tseng, Y.J. 2016. Mutagenicity in a molecule: Identification of core structural features of mutagenicity using a scaffold analysis. PLoS ONE. 11(2): e0148900, https://doi.org/10.1371/journal.pone.0148900.

[39] Prisinzano, T.E. 2005. Medicinal Chemistry: A Molecular and Biochemical Approach. Third Edition By Thomas Nogrady and Donald F. Weaver. Oxford University Press, New York. xiii + 649 pp. 16.5 × 23 cm. ISBN 978-0-19-510456 (Paperback). $95.00. J. Med. Chem. 49(11): 3428, https://doi.org/10.1021/jm068018t.

[40] Chen, L., Wang, L., Shion, H., Yu, C., Yu, Y.Q., Zhu, L., *et al*. 2016. In-depth structural characterization of Kadcyla® (ado-trastuzumab emtansine) and its biosimilar candidate. mAbs. 7(8): 1210–1223, https://doi.org/10.1080/ 19420862.2016.1204502.